Optics Letters

Resonant frequency doubling of phase-modulation-generated few-frequency fiber laser

Xin Zeng,[1,2] Shuzhen Cui,[1,2,4] Xin Cheng,[1,2] Jiaqi Zhou,[1] Weiao Qi,[1,2] and Yan Feng[1,2,3,*]

[1]Shanghai Institute of Optics and Fine Mechanics, Chinese Academy of Sciences, and Shanghai Key Laboratory of Solid State Laser and Application, Shanghai 201800, China
[2]Center of Materials Science and Optoelectronics Engineering, University of the Chinese Academy of Sciences, Beijing 100049, China
[3]Hangzhou Institute for Advanced Study, University of Chinese Academy of Sciences, Hangzhou 310024, China
[4]e-mail: cuishuzhen@siom.ac.cn
*Corresponding author: feng@siom.ac.cn

Received 26 June 2020; revised 2 August 2020; accepted 3 August 2020; posted 3 August 2020 (Doc. ID 401348); published 1 September 2020

Resonant frequency doubling of periodically phase-modulated single-frequency fiber laser is investigated as a method for power scaling of visible fiber lasers. Sinusoidal phase modulation is applied to generate few-frequency lasers at 1064 nm in the proof of principle experiments. By adjusting the modulation frequency to match the free spectral range of a doubling cavity, a resonant enhancement condition can be achieved and a near 30 W 532 nm laser is generated with a maximum conversion efficiency above 80%. The indistinguishable conversion efficiencies between the single-frequency and few-frequency cases prove the feasibility of the approach. Interesting spectral evolvement of the phase-modulated laser in second-harmonic generation is analyzed theoretically and observed in the experiment.

https://doi.org/10.1364/OL.401348

High-power, continuous wave (CW), narrow-linewidth visible lasers have many applications in the scientific and industrial fields, such as pumping titanium sapphire [1,2] or dye laser, deep-ultraviolet laser generation [3,4], laser-guide-star [5–7], semiconductor processing [8], atom trapping, cooling and state manipulation [9–11], and so on. The general methods of obtaining a visible laser are second-harmonic generation (SHG) of diode-pumped solid-state lasers, optically pumped semiconductor lasers, and fiber lasers. Fiber lasers are promising for high-power CW laser generation due to their geometrical advantage in thermal management. For SHG of fiber lasers, a single-pass scheme with periodically poled nonlinear crystals is convenient, but the output power is limited by the low damage threshold of the crystals and thermal dephasing. Lithium triborate (LBO) has a much higher damage threshold and thermal performance, but also has a lower nonlinear coefficient. One solution is to utilize an external resonantly-enhanced cavity with LBO crystals to achieve high-power SHG [3–5,10–13]. By this technique, Tobias Meier *et al.* obtained a 130 W single-frequency CW green laser with a conversion efficiency of 90% [12].

However, single-frequency fundamental lasers were required in external cavity SHG for efficient laser injection and resonant enhancement. For single-frequency fiber lasers, the output power is limited by stimulated Brillouin scattering (SBS) [14,15]. Various techniques have been studied to suppress SBS, such as imposing thermal [16] or strain distribution [17], designing special active fibers [18], using large core size [19] and highly doped active fibers, [20] and so on. Phase modulation is an elegant approach for SBS suppression by expanding the linewidth and reducing spectral power density in a highly controllable way [15,21–24]. But after phase modulation, the laser output is not single frequency anymore. We propose to use a periodically phase-modulated fundamental laser for resonant cavity SHG. A single-frequency laser can be converted to a multiple-frequency laser after periodical phase modulation, and the frequency spacing equals to the fundamental modulation period. When the frequency spacing is equal to one or an integer multiple of the free spectral range (FSR) of the SHG cavity, the resonant enhancement condition should be achievable. This approach, if proved, paves a way for power scaling of frequency-doubled lasers.

In this Letter, we report a demonstration of high-power high-efficient cavity-enhanced SHG with a phase-modulated few-frequency master oscillator fiber power amplifier for the first time. Simple sine-wave phase modulation is applied to generate a few-frequency fundamental laser at 1064 nm. By adjusting the modulation frequency to match the FSR of the doubling cavity, the resonant enhancement condition is achieved after cavity locking. An up to 30 W 532 nm laser is generated with a maximum conversion efficiency above 80%, which is not distinguishable with the single-frequency case. The results prove the feasibility of this approach. Interesting spectral evolvement of the phase-modulated laser in SHG is discussed theoretically and observed in the experiment.

The schematic diagram of the experimental setup is shown in Fig. 1. The few-frequency laser source is seeded by a 1064 nm

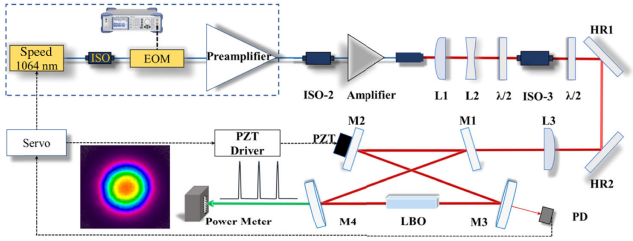

Fig. 1. Schematic diagram of the experimental setup for resonant cavity SHG of a phase-modulated few-frequency fiber laser. The far-field beam profile of the 532 nm laser is also shown.

single-frequency laser with an output of 30 mW and an FWHM spectral width <100 kHz according to the manufacturer, which is protected by a fiber isolator (ISO), phase-modulated by an electro-optical modulator (EOM), and amplified by a preamplifier to 2 W. Then it is further amplified to 40 W in a boost stage with linearly polarized output. The output beam is compressed to a beam diameter of 1.1 mm by a lens pair. A space ISO-3 is used to protect the amplifier. Two half-wave plates are placed before and after the ISO-3 to manipulate the polarization of the high-power 1064 nm laser for proper optical isolation and nonlinear optical conversion. The beam is mode matched to the resonant cavity with a plano-convex lens L3 ($f = 300$ mm). Resonant frequency-doubling cavity has a bow-tie configuration, consists of two concave mirrors (ROC = 50 mm), and contains two flat mirrors with 12° angles of incident. The input coupler M1 is partially reflective of 85% at 1064 nm optimized for impedance matching. The other cavity mirrors, M2, M3, and M4, are high-reflection coated at 1064 nm. M4 is anti-reflection coated at 532 nm. A piezoelectric transducer (PZT) is attached to mirror M2 to adjust the cavity length for active cavity locking. An AR-coated LBO crystal (cut at $\theta = 90°, \varphi = 0°$) with dimensions of $3 \times 3 \times 30$ mm^3 is placed inside the cavity in an oven with ±0.01°C stability. The cavity round-trip length is 164 mm, corresponding to an FSR of 1.646 GHz taking into account the optical length of the LBO crystal. The resonator fundamental mode waist is slightly oval ($\omega_y = 54$ μm, $\omega_x = 50.4$ μm) at the crystal center, which is slightly larger than the optimized waist of 33.5 μm according to Boyd–Kleinman theory [25]. The crystal is thermally tuned to satisfy the non-critical phase-matching condition.

Sinusoidal modulation is used in the experiments for simplicity, because for this type of modulation, the resulting power spectral density of the optical field can be described in an analytical form [23]. The electric field E_ω of the fundamental laser in this case is

$$E_\omega = E_0 \exp[i(\omega t + \gamma \sin \Omega t)]$$

$$= E_0 \sum_{n=-\infty}^{\infty} J_n(\gamma) \exp[i(\omega + n\Omega)t], \quad (1)$$

where γ is the modulation depth, Ω is the modulation frequency, and E_0 is the amplitude. So, after phase modulation, sidebands are generated at both side of the carrier wave ω. The power spectral density (PSD) of the nth sideband is given as follows:

$$P_n \propto J_n^2(\gamma), \quad (2)$$

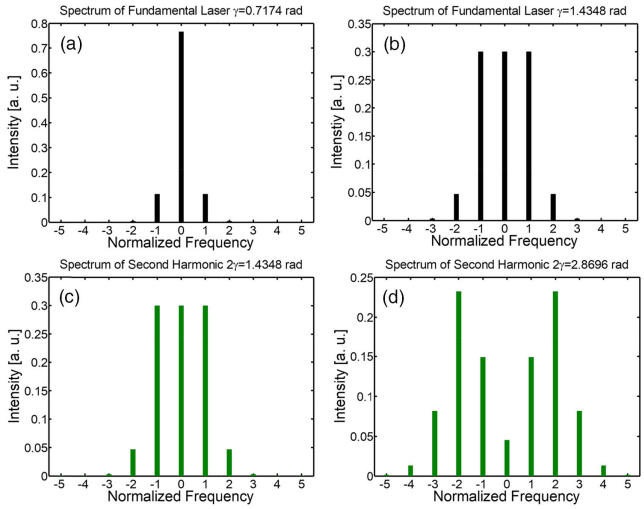

Fig. 2. PSDs of a sinusoidal phase-modulated single-frequency fundamental laser with (a) $\gamma = 0.7174$ and (b) $\gamma = 1.4348$. (c) and (d) are for the corresponding frequency-doubled laser. The frequency shift is normalized with the modulation frequency.

where J_n is the nth order Bessel function of the first kind. The power distribution among the carrier wave and sidebands varies with the modulation depth of EOM, which is determined by the radio frequency (RF) drive power.

We are particularly interested in the spectrum of the frequency-doubled laser. The electric field $E_{2\omega}$ of the frequency-doubled laser has a quadratic dependence on the fundamental laser electric field E_ω:

$$E_{2\omega} \propto E_0^2 \exp[i(2\omega t + 2\gamma \sin \Omega t)]$$

$$\propto E_0^2 \sum_{n=-\infty}^{\infty} J_n(2\gamma) \exp[i(2\omega + n\Omega)t]. \quad (3)$$

Therefore, a factor of 2 in modulation depth increase is predicted for the frequency-doubled laser to the fundamental laser.

With formulas (1) and (3), the PSDs of the fundamental laser and second harmonic with typical modulation depths γ in radian are calculated and shown in Fig. 2. With increasing γ, the intensity of the sidebands increases, and more and more sidebands are generated. At $\gamma = 1.4348$, the first-order sidebands reach the same level as the carrier wave, so the laser power is distributed equally in three frequency components which is good for SBS suppression. After frequency doubling, the carrier wave would, in fact, be reduced. The laser power is distributed to the sidebands with a maximum at the two second-order sidebands. For frequency-doubled lasers, a flat three-line spectrum can be achieved when the modulation applied on the fundamental laser has a depth of $1.4348/2 = 0.7174$.

To achieve resonant enhancement, the first thing is to make sure that the frequency spacing of the phase-modulated laser matches with the FSR of the SHG cavity. It is achieved by finely adjusting the frequency of the RF signal while monitoring the transmission signal from the scanning SHG cavity. When the frequency spacing does not match the FSR, multiple lines are observed. When they match perfectly, these lines merge together and generate a highest transmission signal.

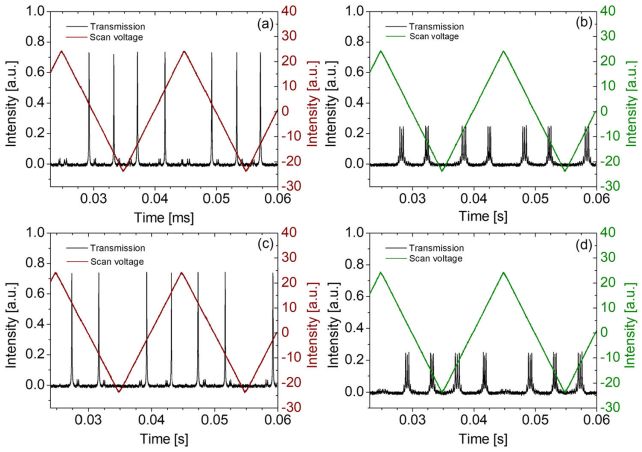

Fig. 3. Transmission signals from the doubling cavity in the cases of (a) a single-frequency laser and phase-modulated laser with RF frequency of (b) 1.546 GHz, (c) 1.646 GHz, and (d) 1.746 GHz, respectively.

Figure 3 shows the transmission signal under different conditions. The transmission signal for a single-frequency case (without phase modulation) is shown in Fig. 3(a) for comparison. The distance between the two lines within the one-way scan is the FSR of the doubling cavity. A modulation depth γ of ~1.4348 (achieved with an RF power of 23.2 dBm) is applied in other measurements in Figs. 3(b)–3(d). When the modulation frequency is off resonance with the cavity, the transmission lines are about one-third of that for the single-frequency case. When the modulation frequency matches with the cavity, the height of the transmission line increases to the same as that for the single-frequency case. The matching modulation frequency is found to be 1.646 GHz, which means the FSR of the doubling cavity is 1.646 GHz in the experiments.

The doubling cavity is then locked to the laser with the Pound–Drever–Hall (PDH) technique [26]. To do this, another RF signal at 25 MHz is applied directly to the single-frequency seed laser, which generates another set of weak sidebands besides the 1.646 GHz spacing sidebands. The 25 MHz sidebands are used to lock the cavity. The resonant laser is detected by a photodetector, amplified, and demodulated with the local 25 MHz oscillator to obtain a dispersive PDH error signal. The error signal is sent to a proportion integration differentiation (PID) controller, whose output is fed back to the piezo driver to stabilize the cavity length. We find that the PDH locking works smoothly with the phase-modulated laser.

After successful resonant frequency doubling, the spectra of the fundamental laser and corresponding second harmonic are investigated with two Fabry–Perot Interferometers (FPIs) of 4 GHz FSR for different spectral ranges. Figures 4(a) and 4(b) show the results for the single-frequency case. Figures 4(c) and 4(d) correspond to the situation in Figs. 2(a) and 2(c) with a modulation depth γ of ~0.7174, where the second harmonic has a flat three-line spectrum. Figures 4(e) and 4(f) correspond to the situation in Figs. 2(b) and 2(d) with a modulation depth γ of ~1.4348, where the fundamental laser has a flat three-line spectrum, and the second harmonic has many more spectral lines. Figures 4(g) and 4(h) show the results at maximum phase modulation possible (~1.763) with our RF signal generator (25 dBm), just to show that the arbitrary phase-modulation

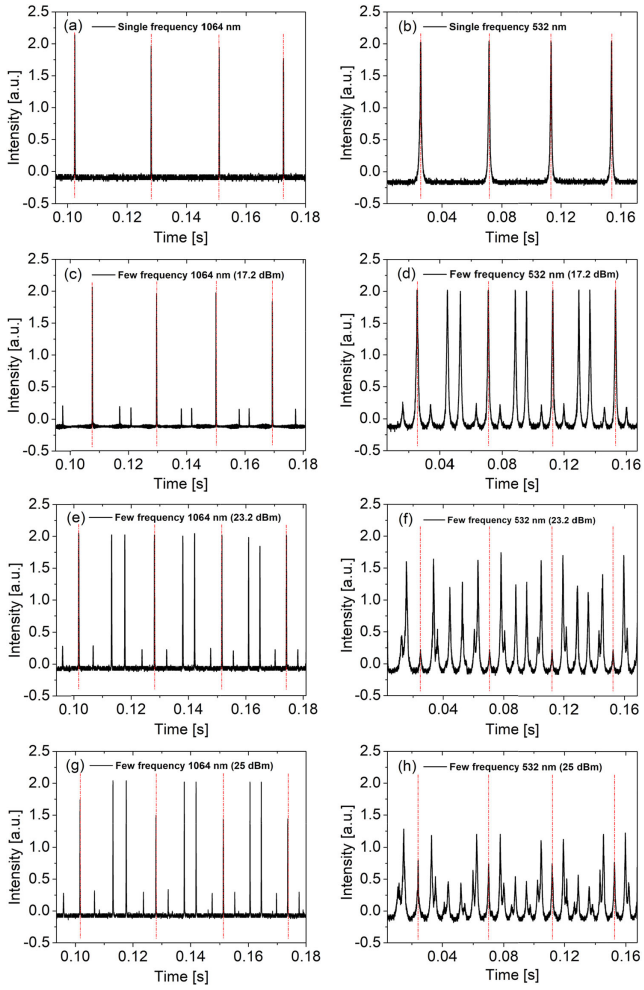

Fig. 4. Spectral analysis of the fundamental laser and corresponding second harmonic with two 4 GHz FPIs. (a) and (b) are for the case of single frequency; (c) and (d), (e) and (f), (g) and (h) are for the cases of different phase-modulation depths as described in the text. Red dotted lines indicate the location of carrier wave.

depth is fine. The experimental results match well with the calculation shown in Fig. 2. The FPI signal lines for the second harmonic are much broader than that of the fundamental laser, because the FPI used for the second harmonic has lower finesse at 532 nm. It cannot resolve the linewidth.

The output power and conversion efficiency of the SHG for the phase-modulated few-frequency laser are measured and compared with the single-frequency case and shown in Fig. 5. The power and efficiency curves almost overlap with each other within the uncertainty of alignment. In all cases, the efficiencies go to a maximum of >80% at a fundamental laser power around 20 W. A further increase in the laser power leads to a drop in conversion efficiency due to the thermal lens effect with the biggest contribution from the optical ISO. A fine realignment or replacement of the mode-matching lens can solve the problem and shift the efficiency maxima to a higher laser power. At maximum fundamental laser power, the second-harmonic powers are 27.76 W, 28.45 W, 29.2 W, and 29.72 W for single-frequency and few-frequency cases shown in Fig. 4, respectively, with conversion efficiencies of 70.7%, 72.47%, 74.38%, and 75.8%. The increase in efficiency with respect to

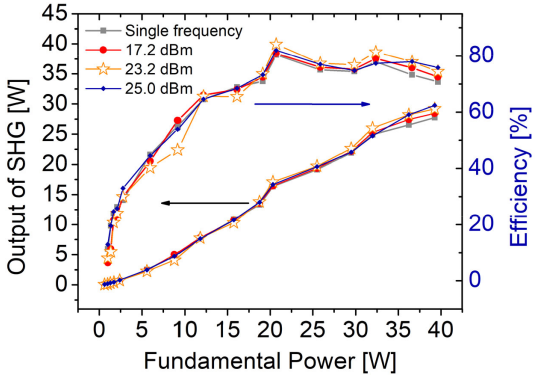

Fig. 5. Output and conversion efficiency of SHG for the cases of single-frequency and few-frequency with RF driver power of 17.2 dB, 23.2 dB, and 25 dB, respectively.

phase-modulation depth at the highest power suggests a suppression of SBS due to phase modulation. Indeed, although the fiber amplifier can work at about 40 W, SBS light starts to appear with single-frequency seed. The phase modulation suppresses the SBS completely. The effect of SBS suppression will be more obvious at higher power, as numerous studies have shown.

The phase-matching bandwidth of the 30 mm LBO crystal used in the experiments is about 300 GHz, and the bandwidth of the phase-modulated laser is only ~3 GHz. Therefore, SHG efficiency is not affected. The power scaling potential of the present technique may be ultimately limited by the crystal acceptance bandwidth. In terms of SHG acceptance bandwidth, 100 times suppression of SBS and power scaling of visible laser power seem possible. In practice, however, the power scaling would be limited first by the technical issues in electro-optical modulation and power handling of the setup.

The far-field beam profile of frequency-doubled few-frequency laser is measured. The result at 25.2 W at an RF power of 17.2 dB is shown in Fig. 1, which has a Gaussian shape as expected.

For common multimode but narrow-linewidth lasers, the SHG efficiency is higher than that of single-frequency lasers [27]. Sum-frequency mixing between modes enhances the efficiency of multimode SHG. It is interesting to note that, for the studied few-frequency laser generated by phase modulation, such an enhancement effect does not exist. This can be understood intuitively considering the fact that the few-frequency laser generated by phase modulation is still single frequency at any moment. There is no sum-frequency mixing possible.

In summary, high-power SHG near 30 W is obtained by utilizing resonant frequency doubling of phase-modulation-generated few-frequency fiber lasers. The output power and conversion efficiency of the few-frequency SHG are shown identical to the single-frequency case. The effective modulation depth of the generated few-frequency second harmonic is exactly twice that applied to the fundamental laser, which agrees well with the theoretical analysis. Sinusoidal modulation is applied in the experiments for simplicity of explanation, but any periodical phase modulation is feasible, including the widely used pseudo-random binary sequence modulation. Since phase modulation is commonly used in high-power narrow-linewidth fiber amplifiers for SBS suppression, resonant frequency doubling of phase-modulation-generated few-frequency fiber lasers is an interesting approach for further power scaling of visible fiber lasers.

Funding. National Key Research and Development Program of China (2018YFB0504600, 2018YFB0504602); Science and Technology Commission of Shanghai Municipality (19441909800).

Disclosures. The authors declare no conflicts of interest.

REFERENCES

1. M. Tawfieq, A. K. Hansen, O. B. Jensen, D. Marti, B. Sumpf, and P. E. Andersen, IEEE J. Quantum Electron. **54**, 1 (2018).
2. G. K. Samanta, S. Chaitanya Kumar, K. Devi, and M. Ebrahim-Zadeh, Opt. Lasers Eng. **50**, 215 (2012).
3. R. Zhao, X. Fu, L. Zhang, S. Fang, J. Sun, Y. Feng, Z. Xu, and Y. Wang, Appl. Opt. **56**, 8973 (2017).
4. T. Südmeyer, Y. Imai, H. Masuda, N. Eguchi, M. Saito, and S. Kubota, Opt. Express **16**, 1546 (2008).
5. L. Zhang, H. Jiang, S. Cui, J. Hu, and Y. Feng, Laser Photon. Rev. **8**, 889 (2014).
6. X. Yang, O. Kitzler, D. J. Spence, Z. Bai, Y. Feng, and R. P. Mildren, Opt. Lett. **45**, 1898 (2020).
7. Y. Lu, L. Zhang, X. Xu, H. Ren, X. Chen, X. Wei, B. Wei, Y. Liao, J. Gu, F. Liu, L. Xu, J. Wang, T. Chen, M. Wan, W. Zhang, C. Tang, and G. Fan, Opt. Express **27**, 20282 (2019).
8. N. Hay, I. Baker, Y. Guo, S. Bashford, and Y. Kwon, Proc. SPIE **8235**, 82351E (2012).
9. A. Mugnier, M. Jacquemet, E. Le Mercier, R. Lebref, and D. Pureur, Proc. SPIE **8237**, 82371F (2012).
10. M. Kwon, P. Y. Yang, P. Huft, C. Young, M. Ebert, and M. Saffman, Opt. Lett. **45**, 339 (2020).
11. H. Z. Chen, X. P. Liu, X. Q. Wang, Y. P. Wu, Y. X. Wang, X. C. Yao, Y. A. Chen, and J. W. Pan, Opt. Express **26**, 33756 (2018).
12. T. Meier, B. Willke, and K. Danzmann, Opt. Lett. **35**, 3742 (2010).
13. S. Cui, L. Zhang, H. Jiang, and Y. Feng, Chin. Opt. Lett. **15**, 041402 (2017).
14. A. Kobyakov, M. Sauer, and D. Chowdhury, Adv. Opt. Photon. **2**, 1 (2010).
15. Y. Aoki, K. Tajima, and I. Mito, J. Lightwave Technol. **6**, 710 (1988).
16. J. Hansryd, F. Dross, M. Westlund, P. A. Andrekson, and S. N. Knudsen, J. Lightwave Technol. **19**, 1691 (2001).
17. L. Zhang, S. Cui, C. Liu, J. Zhou, and Y. Feng, Opt. Express **21**, 5456 (2013).
18. S. Gray, A. Liu, D. T. Walton, J. Wang, M. J. Li, X. Chen, A. B. Ruffin, J. A. DeMeritt, and L. A. Zenteno, Opt. Express **15**, 17044 (2007).
19. F. Beier, C. Hupel, J. Nold, S. Kuhn, S. Hein, J. Ihring, B. Sattler, N. Haarlammert, T. Schreiber, R. Eberhardt, and A. Tünnermann, Opt. Express **24**, 6011 (2016).
20. D. Engin, W. Lu, M. Akbulut, B. McIntosh, H. Verdun, and S. Gupta, Proc. SPIE **7914**, 791407 (2011).
21. Q. Chu, Y. Shi, J. Wen, L. Ouyang, L. Zhao, J. Wang, H. Lin, F. Jing, and C. Tang, Laser Phys. **29**, 055103 (2019).
22. X. Zhao, Y. Yang, H. Shen, X. Chen, G. Bai, J. Zhang, Y. Qi, B. He, and J. Zhou, High Power Laser Sci. Eng. **5**, e31 (2017).
23. C. Zeringue, I. Dajani, S. Naderi, G. T. Moore, and C. Robin, Opt. Express **20**, 21196 (2012).
24. B. Anderson, A. Flores, R. Holten, and I. Dajani, Opt. Express **23**, 27046 (2015).
25. G. Boyd and D. A. D. Kleinman, J. Appl. Phys. **39**, 3597 (1968).
26. E. D. Black, Am. J. Phys. **69**, 79 (2001).
27. M. Jacquemet, D. Harnois, A. Mugnier, and D. Pureur, Proc. SPIE **7914**, 79142C (2011).